Electronic Spectra and Configuration Interaction of Tm 3+ in TmCl 6 3−

ARTICLE *in* THE JOURNAL OF PHYSICAL CHEMISTRY A · JUNE 2004

Impact Factor: 2.69 · DOI: 10.1021/jp049471o

3 AUTHORS, INCLUDING:

Peter Anthony Tanner
The Hong Kong Institute of Education

355 PUBLICATIONS **4,367** CITATIONS

SEE PROFILE

Electronic Spectra and Configuration Interaction of Tm^{3+} in $TmCl_6^{3-}$

Michèle D. Faucher,† Peter A. Tanner,*,‡ and Chris S. K. Mak‡

88 Avenue Jean Jaurès, 92140 Clamart, France, and Department of Biology and Chemistry, City University of Hong Kong, Tat Chee Avenue, Kowloon, Hong Kong SAR. P.R. China

Received: February 5, 2004; In Final Form: April 13, 2004

Low-temperature electronic absorption and emission data are reported for Tm^{3+} at the octahedral site in crystals of $Cs_2NaTmCl_6$. Thirty-seven crystal field levels (total degeneracy 88) of the f^{12} configuration (total degeneracy 91) have been assigned, and in several cases the levels are split due to electron−phonon coupling interactions. The fitting of the energy levels, using the conventional f^{12} analysis with 12 variable parameters, gives a mean deviation of 53.3 cm^{-1}. This is reduced to 9.3 cm^{-1} by including the $4f^{12}np^6/4f^{13}np^5$ configuration interaction, using 16 variable parameters. The results indicate a tendency for the early members in the series of Ln^{3+} ions to interact with the p-electron, and the later members with the p-hole, configurations, following the redox properties of the ions. The interacting configuration is charge-transfer ($n = 3$) rather than metal ion ($n = 5$), and the mixing of ligand wave functions with those of the metal ion may be responsible for the unusually strong electron−phonon coupling identified for several electronic states of Tm^{3+} in $TmCl_6^{3-}$.

Introduction

The energy levels of lanthanide ions in the crystalline hexachloroelpasolite system[1] are simpler than for Ln^{3+} diluted into other crystals because the octahedral site symmetry gives rise to high degeneracies of electronic levels. Several systematic energy level parametrizations have been carried out for the entire series of lanthanide ions with general overall success, but with some notable discrepancies.[2−4] Although the *SL*-term-dependence of the crystal field parameters has been recognized for some time, attempts to explain "anomalous" multiplet splittings using two-electron operators have not proved to be conclusive.[5,6] More recent parametrizations have utilized larger datasets, including energy levels deduced from two-photon spectroscopy. Evidence was reported for electron correlation induced by the crystal field,[7] yet until recently the comparisons of experimental versus calculated energy level listings have been those from calculations involving one-electron crystal field operators.[8−12] A recent paper by Thorne et al.[13] shows that improvement can be obtained by adding the spin-correlated crystal field to the normal crystal field. Some discrepancies remain, however, and a detailed account of correlation crystal field analysis for $Cs_2NaTbBr_6$ is given in ref 14. From our previous studies, we have found that the inclusion of $4fmp^1$ configuration interaction into the parametrization of the $4f^2$ energy level scheme decreases the mean deviation of the fit using the single configuration $4f^2$ alone by a factor of 2.9 (i.e., from 32.7 to 11.6 cm^{-1}).[15a] The interaction is most marked for the $^1G_4$ and $^1D_2$ multiplets of Pr^{3+}, since large crystal field off-diagonal matrix elements between these terms and certain singlet terms of the $4fmp^1$ configuration perturb the crystal field levels of these $4f^2$ multiplet terms. Using the same method, for another elpasolite compound $Cs_2NaErCl_6$, the mean deviation for 75 levels (with a total degeneracy of 130) was reduced from 21.4 to 10.5 cm^{-1}.[15b]

The objective of the present study is to see if the interaction with excited configurations is equally important for the f^{12} ion Tm^{3+}. Crude point charge calculations predict a decrease in crystalline field across the lanthanide series.[2] In the cubic elpasolites $Cs_2NaLnCl_6$, the lattice parameters are 1091 and 1069 pm for Ln = Pr and Ln = Tm, respectively,[16] so that the Tm−Cl distance is shorter. However the radial integrals $\langle r^k \rangle$ are smaller for Ln = Tm so that overall the crystal field experienced by Tm^{3+} is weaker. Slater parameters are expected to scale linearly with atomic number, so that the effects of higher metal ion configurations may be less important in perturbing $4f^{12}$ levels than $4f^2$ levels. However, the nature of the interacting configuration mp^M has not been clear in previous cases because its energy seems to be anomalously low for metal-centered configurations.[15a,b,17] Evidence from the energy level datafit of Er^{3+} strongly suggests that the equiparity interacting configuration is a charge-transfer configuration.[15b]

Several previous studies have been concerned with the electronic spectra of Tm^{3+} in octahedral symmetry. The absorption and magnetic circular dichroism spectra were reported by Schwartz et al.,[18] who assigned 12 crystal field levels. Subsequent reports of the absorption and emission spectra[19,20] were not in agreement and remained unresolved.[21] An alternative relativistic calculation approach was equally unsatisfactory.[22] One of the problematic terms was the electronic ground state, $^3H_6$, where an apparent discrepancy between experiment and calculation of ca. 100 cm^{-1} existed for the Γ_2 (A_{2g}) crystal field level. (Since all of the electronic levels of the f^{12} configuration are of even parity, we omit the crystal field level irrep label g throughout). Amberger et al.[23] had previously commented on the unusual behavior in the electronic Raman spectrum of $Cs_2NaTmCl_6$, and this was subsequently reinvestigated by Tanner et al.[24] Two energy levels (at 108 and 148 cm^{-1} at 10 K) were found to be derived from the $^3H_6a\Gamma_5$ (T_{2g}) crystal field level, through the electron−phonon coupling interaction of the vibronic level $^3H_6\Gamma_1 + \nu_5(\tau_{2g})$ and the electronic level $^3H_6a\Gamma_5$. From the observation of a hot electronic Raman transition, the Γ_2 (A_{2g}) level was reassigned near the

* To whom correspondence should be addressed. E-mail: (P.A.T.) bhtan@cityu.edu.hk, (M.D.F.) faucher.michele@free.fr.

† 88 Avenue Jean Jaurès.

‡ City University of Hong Kong.

10.1021/jp049471o CCC: $27.50
Published on Web 05/20/2004

calculated energy.[24] A closer agreement with calculation was then found when the estimated unperturbed $^3H_6a\Gamma_5$ energy was utilized in the energy level parametrization.[4] Further evidence for electron−phonon coupling of the $^3H_6a\Gamma_5$ level has recently been put forward from a high pressure study.[25] However, these phenomena were not considered in the two-photon study of the energy levels between 27 000 and 36 000 cm^{-1},[13] where the $^3H_6a\Gamma_5$ level was assigned at 148 cm^{-1}. Assignments were not forthcoming for some spectral features, which led to some differences in the proposed energy level scheme from that in the present study. From the $^3P_2$ emission spectrum of $TmCl_6^{3-}$,[26] an apparent "doubling" of a certain crystal field level (in this case, in the excited $^3H_4$ term of Tm^{3+}) has also been found. Again, the perturbation arises from the coupling of an electronic level with an even-parity vibronic level, and the estimated unperturbed energy level lies much closer to the calculated position.

After a brief review of experimental details and the requisite structural and vibrational data, the results from the reinvestigation and extension of the emission and absorption spectral data are analyzed. A critical comparison with results from two-photon spectra is then made. Finally, the energy level dataset is compared with the results of calculations using the $4f^{12}$ model alone and with those involving interaction with excited configurations. We have also made investigations of the electronic spectra of $Cs_2LiTmCl_6$ and Cs_2LiYCl_6:Tm. The vibrational behaviors of these systems differ from that of $Cs_2NaTmCl_6$, leading to differences in the vibronic sidebands of the electronic spectra. The results served to confirm the assignments of the electronic energy levels, but we do not present them since the spectra were generally not of such high quality.

Experimental, Structural, and Vibrational Data

From inelastic neutron scattering measurements, Knudsen et al.[27] found that $Cs_2NaTmCl_6$ retains the cubic *Fm*3*m* structure between room temperature and 10 K. Evidence for a small tetragonal distortion in $Cs_2NaTmCl_6$ was reported[28] from enhanced ^{169}Tm nuclear magnetic resonance measurements at 4.2 K. This distortion evidently results in the splitting of the $^3H_6\Gamma_4$ level, assigned at 58 cm^{-1},[28] by 1 or 2 cm^{-1}. Our measurements were carried out at 10 K or above, so that the cubic structure is preserved.

$Cs_2NaTmCl_6$ was prepared as polycrystalline material by Morss method E,[1,19] but HCl gas was passed over the powders of $Cs_2LiTmCl_6$, Cs_2LiYCl_6:Tm at 420 °C for 3 days prior to passage through the Bridgman furnace. (Unpublished) absorption spectra were recorded some years ago, between 1992 and 1995, using a Biorad FTS-60A spectrometer between 300 and 10 K, at a resolution of 2 cm^{-1} in the region from 4000 to 39 000 cm^{-1}, using quartz−halogen, xenon, and deuterium lamps. In 2001, the region above 25 000 cm^{-1} was reinvestigated using deuterium and xenon lamp sources, an Acton 0.5 m monochromator with an 1800 g mm^{-1} grating blazed at 250 nm, and a back-illuminated SpectruMM CCD detector. The latter spectra were not background corrected. The sample was housed in an Oxford Instruments closed cycle cryostat, with base temperature 10 K. The spectral energies were converted to vacuum wavenumbers. The absolute calibrations in the ultraviolet region were found to vary by ca. ±5 cm^{-1} for our spectra recorded at different times, presumably due to the refractive index assumption when converting to vacuum wavenumbers. Otherwise, the electronic level energies deduced from absorption spectra are generally accurate to ±2 cm^{-1} when zero phonon lines are directly observed, or $<\pm 4$ cm^{-1} when inferred from vibronic structure.

TABLE 1: Vibrational Data for $Cs_2NaTmCl_6$ at 10−20 K

normal mode of $TmCl_6^{3-}$ [a]	unit cell group mode[a,b]	Raman spectrum (cm^{-1})	components in vibronic spectra (cm^{-1})
ν_1, α_{1g}, Tm-Cl sym str	S_1	296	
ν_2, ϵ_g, Tm-Cl sym str	S_2	237	
	S_3 τ_{1g} rot.		
	S_5 Cs^+ str	47	47
ν_3, τ_{1u}, Tm-Cl asym str	S_6		245, 260, 288
ν_4, τ_{1u}, Cl-Tm-Cl b	S_7		111, 133
ν_5, τ_{2g}, Cl-Tm-Cl b	S_4	130[c]	
	S_8 Na^+ str		182
	S_9 Cs^+ transl		60, 68
ν_6, τ_{2u}, Cl-Tm-Cl b	S_{10}		78, 88

[a] Key: sym, symmetric; str, stretch; asym, antisymmetric; b, bend; rot., rotatory mode; trans, translatory mode. [b] Reference 29. [c] At 300 K.

Low-temperature emission spectra of $Cs_2NaTmCl_6$ were recorded at the University of Hong Kong and the equipment setup has previously been described.[26]

Vibrational data for $Cs_2NaTmCl_6$ are available for the gerade modes from low-temperature Raman spectra,[24] and for the ungerade modes from the vibronic sidebands of the optical spectra at low temperature.[19] The latter spectra show dispersion and transverse-longitudinal mode splittings so that multiple structure is observed for each internal moiety mode. Table 1 summarizes this and includes the energies of the unit cell group modes due to Na^+ and Cs^+ motions also. Also presented are the moiety-mode and unit cell group notations for the vibrations which are employed in this work. The derived energy levels of $Cs_2NaTmCl_6$ are listed in the expt column in Table 2, and the rationale for assignments is now discussed.

Results and Discussion

The electronic ground state of Tm^{3+} in $Cs_2NaTmCl_6$ is $^3H_6\Gamma_1$. An overview of the energy levels of this system is provided in Figure 1. The one-photon absorption spectra from this initial state are characterized by electric-hexadecapole ($\Gamma_1 - \Gamma_1$), electric-quadrupole ($\Gamma_1 - \Gamma_3$ or $\Gamma_1 - \Gamma_5$), or magnetic-dipole allowed ($\Gamma_1 - \Gamma_4$) zero phonon lines, with associated vibronic sidebands. The hexadecapole and electric-quadrupole electronic origins are generally indistinguishable from very weak, sharp, coincident electric-dipole allowed bands arising from Tm^{3+} ions situated at defect sites. Accordingly, the oscillator strengths of the $^3H_6\Gamma_1 \rightarrow {}^3F_4\Gamma_5$, $^3H_4\Gamma_5,\Gamma_3$, $^1G_4\Gamma_5$ electric-quadrupole allowed transitions were all measured to be at least 1 order of magnitude greater than the calculated oscillator strengths.[30] The magnetic dipole (MD) zero phonon lines are intense in some cases, particularly for the $\Delta J = 1$, $\Delta L = 1$, $\Delta S = 0$ transition: $^3H_6 \rightarrow {}^3H_5$. Calculated magnetic dipole (MD) oscillator strengths for the eight $^3H_6\Gamma_1 \rightarrow \Gamma_4$ transitions were in reasonable agreement with experiment, except that the calculated values for two most intense transitions (to terminal Γ_4 levels of $^3H_5$ and $^1I_6$) were several times greater than experimental values, and this was attributed to saturation effects, also observed previously in the spectra of Yb^{3+}.[31] The MD oscillator strength of $^3H_6\Gamma_1 \rightarrow {}^3P_1\Gamma_4$ was calculated (using the eigenvectors from the f^{12} calculation) about 2 orders weaker than that measured from the assigned feature. However, the calculated value increased by a factor of 20 when the $f^{13}np^5$ eigenvectors were employed, showing the sensitivity of this oscillator strength to the eigenvector composition.

The selection rules operative for the vibronic sidebands produce unique structures for $\Gamma_1 \rightarrow \Gamma_1$ transitions (where only

TABLE 2: Experimental and Calculated Energy Levels of Tm^{3+} in $Cs_2NaTmCl_6$[a,b]

$^{2S+1}L_J$	IR	expt	calc 1: $4f^{12}$	expt − calc	calc 2: SCCF	expt − calc	calc 3: $4f^{12}np^6 + 4f^{13}np^5$	expt − calc
$^3H_6$	Γ_1	0	−96	96	−7	7	−10	10
	Γ_4	56	−13	69	50	6	50	6
	aΓ_5	123[c]	82	41	117	6	118	5
	Γ_2	261	278	−17	243	18	256	5
	bΓ_5	370	439	−69	371	−1	376	−6
	Γ_3	394	473	−79	396	−2	401	−7
$^3F_4$	Γ_5	5547	5486	61	5498	49	5552	−5
	Γ_3	5814	5817	−3	5838	−24	5818	−4
	Γ_4	5859	5888	−29	5891	−32	5865	−6
	Γ_1	5938	5980	−42	5958	−20	5934	4
$^3H_5$	aΓ_4	8240	8201	39	8251	−11	8237	3
	Γ_3	8270	8244	26	8285	−15	8270	0
	Γ_5	8437	8464	−27	8435	2	8441	−4
	bΓ_4	8533	8594	−61	8534	−1	8541	−8
$^3H_4$	Γ_5	12 538	12 497	41	12 526	12	12 546	−8
	Γ_3	12 607	12 642	−35	12 650	−43	12 636	−29
	Γ_4	12 766[d]	12 758	8	12 750	16	12 737	29
	Γ_1	12 880	12 930	−50	12 889	−9	12 882	−2
$^3F_3$	Γ_2	14 470	14 360		14 377		14 418	
	Γ_4	14 428	14 447	−19	14 437	−9	14 427	1
	Γ_5	14 454	14 431	23	14 436	18	14 450	4
$^3F_2$	Γ_3	14 956	14 939	17	14 940	16	14 946	10
	Γ_5	15 130	15 132	−2	15 131	−1	15 132	−2
$^1G_4$	Γ_5	20 852	20 832	20	20 812	40	20 854	−2
	Γ_3	21 357	21 328	29	21 356	1	21 360	−3
	Γ_4	21 426	21 416	10	21 431	−5	21 419	7
	Γ_1	21 507	21 520	−13	21 516	−9	21 503	4
$^1D_2$	Γ_5	27 653	27 638	15	27 705	−52	27 651	2
	Γ_3	27 702	27 707	−5	27 636	66	27 707	−5
$^1I_6$	Γ_3	34 117	34 234	−117	34 133	−16	34 122	−5
	aΓ_5	34 158	34 276	−118	34 184	−26	34 164	−6
	Γ_2		34 424		34 369		34 328	
	bΓ_5	34 822	34 805	17	34 836	−14	34 805	17
$^3P_0$	Γ_1	34 846	34 869	−23	34 856	−10	34 846	0
$^1I_6$	Γ_4	34 983	34 931	52	34 995	−12	34 975	8
	Γ_1	35 196[e]	35 042	154	35 133	63	35 203	−7
$^3P_1$	Γ_4	35 884	35 890	−6	35 866	18	35 889	−5
$^3P_2$	Γ_3	37 462	37 478	−16	37 484	−22	37 451	11
	Γ_5	37 854	37 842	12	37 857	−3	37 864	−10
$^1S_0$	Γ_1		71 591		71 718		75 585	

[a] The parameters of calculations 1−3 are listed in Table 3. [b] IR irreducible representation. Calculated unperturbed energies from observed levels at (in cm^{-1}). [c] 108, 148. [d] 12 693, 12 838. [e] 35 207, 35 184.

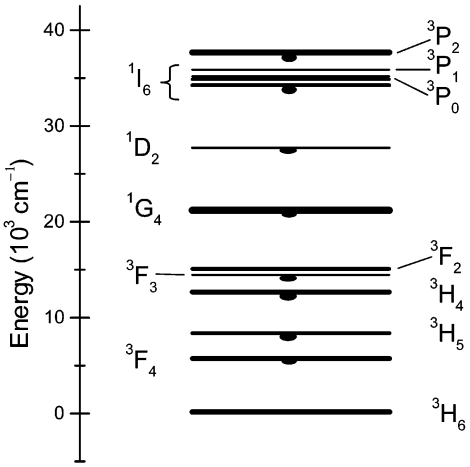

Figure 1. Energy levels of Tm^{3+} in $Cs_2NaTmCl_6$. Luminescent levels are identified.

τ_{1u} modes appear), and $\Gamma_1 \rightarrow \Gamma_2$ transitions (where only the τ_{2u} mode is observed), but otherwise the ν_i ($i = 3, 4, 6$) modes are potentially active for $\Gamma_1 \rightarrow \Gamma_i$ ($i = 3, 4, 5$) transitions (Table 1). Studies of spectra at 30 and 80 K were invaluable in identifying the "hot" bands of electronic transitions.

Emission Spectra of $TmCl_6^{3-}$. Figure 1 shows that low-temperature emission has been observed from all of the excited *SLJ* terms of Tm^{3+} in Cs_2NaYCl_6:Tm and/or $Cs_2NaTmCl_6$,[19,20,26] except for $^3F_2$ and $^3P_{0,1}$, where multiphonon relaxation dominates over the radiative process. However, no previous discussion or interpretation has been given for the emission from $^1D_2$. Since the splitting of the $^1D_2$ crystal field levels is calculated to be $\sim$50 cm^{-1}, low temperature emission is expected only from the lower (Γ_5) level. The strongest transition from the $^1D_2$ term is to $^3F_4$. Figure 2 shows the region in the 10 K emission spectrum of $Cs_2NaTmCl_6$ between 22 100 and 21 100 cm^{-1} under various excitation lines. No emission in this region is evident for excitation lines between 240 and 266 nm, but the dips below the baseline correspond to bands in the absorption spectrum of $Cs_2NaTmCl_6$, which has previously been reported with a much better signal-to-noise ratio.[19a] There is a one-to-one correspondence between the energies and the band numbers marked for the 246 nm excitation in Figure 2, with the energies and band numbers listed in Table 3 of ref 19a. There is one exception, marked T, which is not evident in the absorption spectrum. This dip is coincident with the position of the $^3H_6\Gamma_1 \rightarrow {}^1G_4\Gamma_4$ magnetic dipole allowed zero phonon line. In fact, the "absorption spectra" in Figure 2 occur from Tm^{3+} ions near the crystal surface, rather than in the bulk as in ref 19a, so that defect sites are then more plentiful and defect site zero phonon band intensities are enhanced by the electric dipole mechanism.

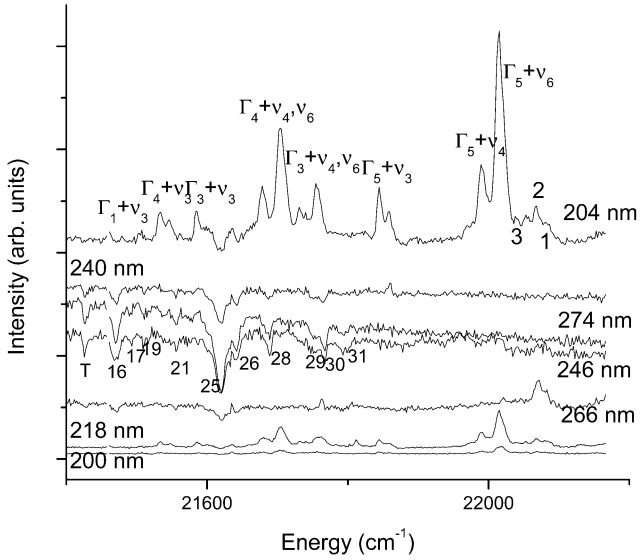

Figure 2. 10 K luminescence spectra of $Cs_2NaTmCl_6$ between 21 400 and 22 160 cm^{-1} under various laser excitation lines. The numbers labeling the dips in the 246 nm excited spectrum are the same as in Table 3 of ref 19a. Peaks in the 204 nm spectrum are labeled according to the terminal $^3F_4$ state. The luminescent state is $^1D_2\Gamma_5$ in all cases. Refer to the text.

TABLE 3: Hamiltonian Parameters of Tm^{3+} in $Cs_2NaTmCl_6$

	value (cm^{-1})		
parameter	calc 1[c]	calc 2[c]	calc 3[c]
F^2	99 725 (134)	99 738 (67)	101 690 (69)
F^4	68 592 (413)	69 625 (215)	71 181 (131)
F^6	48 231 (402)	48 533 (202)	50 609 (95)
α	19.2 (1.3)	18.0 (0.7)	19.0 (0.4)
β	−730 (88)	−729 (47)	−675 (24)
γ	[2716][a]	[2716]	2128 (46)
M^0	[3.38]	[3.38]	4.31(0.5)
P^2	[43]	[43]	461(83)
ζ_f	2616 (7)	2616 (2)	2633 (1)
B_0^4(f, f)	1787 (85)	2203 (63)	453 (52)
B_0^6(f, f)	170 (58)	222 (44)	−119 (16)
c^4(f, f)		−0.42	
c^6(f, f)		−0.33	
ΔE_{avg} (*207 403*)			[38 500]
X (*1*)[b]			0.08 (0.02)
ζ_p (*32 000*)			[1000]
B_0^4(f, p)			−15 389 (298)
N[c]	37	37	37
n[c]	12	14	16
δ[c]	53.3	25.0	9.3
σ[c]	64.8	31.7	12.3

[a] Parameters in square brackets were held constant during the final steps of the refinement. Italic numbers between parentheses are theoretical values of the parameters for an atomic metal-centered configuration. [b] X is a common multiplier of the theoretical R^k values which are in cm^{-1}: R^2(f, p, f, p) = 55 952; R^2(f, p, p, f) = 27 980; R^4(f, p, p, f) = 21 737; R^2(f, f, f, p) = −14 616; R^4(f, f, f, p) = −6554. [c] calc 1 and calc 2 were performed in $4f^{12}$, calc 3 in $4f^{12}5p^6/4f^{13}5p^5$. N is the number of levels, n the number of parameters. δ is the unbarycentered mean deviation, and σ is the standard deviation: $[\sum_{i=1,N}(Ei_{exp} - Ei_{calc})^2/(N - n)]^{1/2}$.

The emission spectra in Figure 2 are clearly excited by wavelengths between 200 and 218 nm, i.e., with excitation into the charge-transfer states of $TmCl_6^{3-}$.[32] However, no charge-transfer emission is detected. The highest energy bands 1, 2, and 3 correspond to the $^3P_2\Gamma_3 \rightarrow {}^3F_2\Gamma_5 + \nu_3$(243, 260, 288) bands[26] superimposed upon lattice mode structure of the $^1D_2\Gamma_5 \rightarrow {}^3F_4\Gamma_5$ transition. The energies of the $^3F_4$ crystal field levels have previously been assigned from absorption[19b] and emission[19b,c,26] spectra, and this enables comprehensive assignments to be made for the 204 nm excited spectrum as shown in Figure 2. These assignments enable the lowest (Γ_5) crystal field level of $^1D_2$ to be assigned at 27 654 ± 3 cm^{-1}.

We have investigated the emission from $^1I_6$ in Cs_2LiYCl_6:Tm, under 199.8 nm excitation and find that it occurs from a level at 34 126 cm^{-1}, assigned herein to Γ_3. No emission was observed in our spectra from $^1I_6$ in neat $Cs_2NaTmCl_6$, but it is evident in the 77 K emission spectrum of $Cs_2NaTm_{0.05}Y_{0.95}Cl_6$ reported by Thorne et al.[13] The cross-relaxation

$$^1I_6\Gamma_4\ (\text{ion 1}) + {}^3H_6\Gamma_1\ (\text{ion 2}) \rightarrow {}^3H_4\Gamma_3\ (\text{ion 1}) + {}^1G_4\Gamma_1\ (\text{ion 2})$$

is resonant and depopulates $^1I_6$ in the neat crystals. Cross-relaxation processes from $^1G_4$ and $^1D_2$ also occur in neat crystals of Cs_2MTmCl_6 (M = Li, Na).[20,33]

The assignments of energy levels below $^1I_6$, and of $^3P_2\Gamma_3$, listed herein are generally confirmed by the emission spectra, and extensive tabulations have previously been given.[19,20] It is noted in particular, however, that the low-temperature emission spectra enable the unambiguous location of the *lowest* crystal field level of each *SLJ* term: for example, the Γ_4 level of $^3F_3$, discussed later.

Absorption Spectra of $Cs_2NaTmCl_6$. Detailed assignments and listings of bands in certain electronic transitions have previously been given[19] so that we summarize the conclusions here and focus upon differences with previous studies.

$^3H_6$ Term. The assignment of crystal field levels in the ground-state term has been made from emission spectra[19,26] and electronic Raman spectra.[24,25] Two levels of mixed $a\Gamma_5$ parentage are located at 108 and 148 cm^{-1}, and we have taken the unperturbed energy to be 123 cm^{-1} in Table 2.[24]

$^3F_4$ and $^3H_5$ Terms. The previous assignments for the $^3F_4$ term were based upon emission measurements and the 20 K absorption spectrum.[19] The $^3H_6 \rightarrow {}^3F_4$ transition is mainly vibronic in character, whereas the $^3H_6 \rightarrow {}^3H_5$ transition is dominated by the intense $\Gamma_1 \rightarrow a\Gamma_4$ magnetic dipole zero phonon line. Assignments for the $^3H_5$ term have been made from the 20 K absorption spectrum.[33] Line positions have been compared with those in Cs_2ZrCl_6:Tm^{3+}.[34] The 10 K spectra of both transitions have recently been utilized[35] for comparison with the calculated vibronic intensities. The energy levels in Table 2 are similar to those previously reported.[19]

$^3H_4$ Term. The assignments for the $^3H_4$ crystal field levels have been made from absorption and emission spectra.[19] However, the Γ_4 level, assigned at 12 840 cm^{-1}, is then far from the calculated location, 12 735−12 760 cm^{-1}.[4] In the $^3P_2$ emission spectra terminating upon $^3H_4$, a further level, at 12 692 cm^{-1}, was identified from intense vibronic structure.[26] The observation of two Γ_4 levels was attributed in an analogous manner to electron−phonon coupling phenomena, just as for the two $a\Gamma_5$ levels in the electronic ground state. In the $^3H_4$ case, the coupling occurs between $\Gamma_5 + \nu_2 = 12\,538 + 237 = 12\,775$ cm^{-1}, and the Γ_4 crystal field level.

A reexamination of the 10 K $^3H_6 \rightarrow {}^3H_4$ absorption spectrum shows that the ν_i (i = 3, 4, 6) structure based on the electronic origin at 12 692 cm^{-1} is largely overlapped by other structure, but that weak bands (at 12 781, 12 804 cm^{-1}) which cannot be assigned to other transitions, can be associated with the ν_6 and ν_4 structure of this electronic transition.

$^3F_2$, $^3F_3$, $^1G_4$ Terms. The assignments for these terms given here are similar to those previously given,[4] with the additional tentative assignment of the $^3F_3\Gamma_2$ level at 14 467 cm^{-1}, from

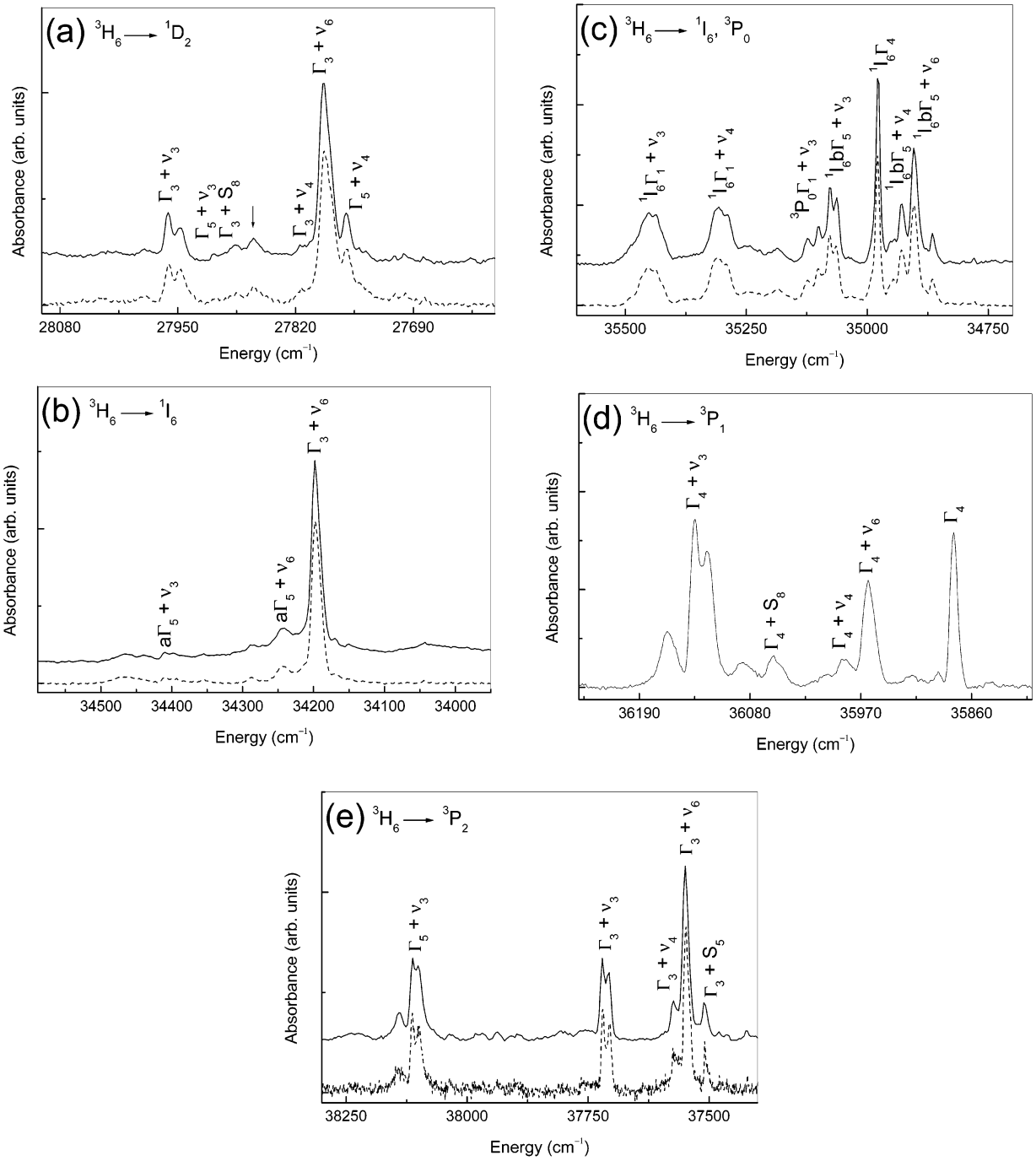

Figure 3. (a−e) 10 K absorption spectra of $Cs_2NaTmCl_6$ between 27 000 and 38 000 cm^{-1}. The assignments of prominent vibronic structure are marked by the terminal crystal field and vibrational levels. The electronic ground state is $^3H_6\Gamma_1$. The spectra were recorded for different crystals using the Biorad FTS (dotted line) and Acton monochromator/CCD (full line).

the $^3P_2$ emission spectrum of $Cs_2NaTmCl_6$. This assignment is consistent with the location of the $^3H_6\Gamma_1 \rightarrow {}^3F_3\Gamma_2 + \nu_6$ vibronic origin in the 10 K absorption spectrum at 14 562 cm^{-1} (i.e., the electronic origin is inferred to be at 14 474 cm^{-1}). The mean value for $^3F_3\Gamma_2$ (14 470 cm^{-1}) is listed in Table 2. The assignments differ from those of Thorne et al.,[13] who interchanged the order of $^3F_3$ Γ_4,Γ_5. From the emission spectrum of $TmCl_6^{3-}$,[19a] it is certain that Γ_4 is the lowest crystal field level of the $^3F_3$ term because emission is observed from this level at low temperature.[19a]

$^1D_2$ Term. The 10 K $^3H_6\Gamma_1 \rightarrow {}^1D_2$ absorption spectrum is shown in Figure 3a, with the prominent vibronic structure identified. One transition is readily located from the intense ν_6 and ν_3 bands, with the electronic origin inferred to be at 27 702 cm^{-1}. Crystals of $Cs_2NaTmCl_6$ were doped with Ce^{3+} to prove that the weaker structure in this region does not correspond to Ce^{3+} impurity. Two bands marked in Figure 3a are then assigned to ν_4 (111 cm^{-1}) and ν_3 (259 cm^{-1}) structures of the $\Gamma_1 \rightarrow \Gamma_5$ transition since the location of the unobserved zero phonon line is inferred to be at 27 652 cm^{-1}, in agreement with the value from the emission spectrum. Two weak bands then remain unassigned in Figure 3a. One of these is reasonably assigned to $\Gamma_1 \rightarrow \Gamma_3 + S_8(186)$, but the vibrational interval of the other band (marked with an arrow in Figure 3a: 214 or 165 cm^{-1}) does not correspond to a fundamental mode of $TmCl_6^{3-}$. An analogous medium-weak unassigned feature is observed in the 10 K absorption spectrum of $Cs_2NaY_{0.9}Tm_{0.1}Cl_6$, where the electronic origins $\Gamma_1 \rightarrow \Gamma_5$ and $\Gamma_1 \rightarrow \Gamma_3$ are inferred to be at

27 653 and 27 702 cm^{-1}, respectively. In the two-photon spectrum of ref 13 (see later), a weak band is observed at 130 cm^{-1} above the $\Gamma_1 \rightarrow \Gamma_5$ transition, which corresponds to ν_5. It is unlikely that the unassigned feature in Figure 3a corresponds to $\Gamma_1 \rightarrow \Gamma_5 + \nu_6 + \nu_5$ because $\Gamma_1 \rightarrow \Gamma_5 + \nu_6$ is not observed. In conclusion, no firm assignment can be made for this band.

$^1I_6$, $^3P_0$, and $^3P_1$ Terms. The transitions to $^1I_6$ crystal field levels overlap those to $^3P_0$ and $^3P_1$, in the spectral region between 33 000 and 36 200 cm^{-1}, and these constitute the most problematic levels to assign. We present a detailed interpretation of the bands in this region, and make extensive use of the spectral changes that occur from 10 to 60 K. Previously, two magnetic dipole transitions were assigned to prominent spectral features,[4] but one of these, $\Gamma_1 \rightarrow {}^1I_6\Gamma_4$, is reassigned herein.

Figsure 3b−d show this spectral region in three parts. At lowest energy, the intense band near 34 205 cm^{-1} was previously assigned to $\Gamma_1 \rightarrow {}^1I_6\,\Gamma_4$, but the observation of a hot band at 173 cm^{-1} to low energy at 30 K, makes the assignment to a ν_6 vibronic origin more likely. The electronic origin is thus inferred to be at 34 117 at 10 K. Energy level calculations show that the lowest energy transition to $^1I_6$ is $\Gamma_1 \rightarrow {}^1I_6\Gamma_3$. At 30 K, the $\Gamma_4 \rightarrow {}^1I_6\Gamma_3$ hot band is observed as a sharp, weak feature at 54 cm^{-1} to low energy of the inferred position of the $\Gamma_1 \rightarrow {}^1I_6\Gamma_3$ electronic origin. However, besides lattice modes, no further structure is associated with the $\Gamma_1 \rightarrow {}^1I_6\Gamma_3$ transition. The medium intensity band at 42 cm^{-1} to higher energy of $\Gamma_1 \rightarrow {}^1I_6\Gamma_3 + \nu_6$ is then assigned to the ν_6 vibronic origin of the next-highest $^1I_6$ transition, $\Gamma_1 \rightarrow {}^1I_6a\Gamma_5$, and the corresponding ν_3 structure is clearly located to higher energy. A broad band near 34 470 cm^{-1} is tentatively associated with the next-highest transition, $\Gamma_1 \rightarrow {}^1I_6\Gamma_2 + \nu_6$, so that the corresponding electronic origin is inferred to be at 34 384 cm^{-1}. The observation of a 30 K hot band at 34 587 cm^{-1}, assigned to $\Gamma_4 \rightarrow {}^1I_6\Gamma_2 + \nu_3$, is consistent with this.

The next group of bands, Figure 3d, is readily assigned to the vibronic structure of an electronic origin, which is observed with medium intensity. This transition is assigned to $\Gamma_1 \rightarrow {}^3P_1\Gamma_4$ on the basis of the magnetic dipole intensity of the zero phonon line and the energy level calculation.

A further three $^1I_6$ levels and one $^3P_0$ level then remain unassigned. The lowest energy bands in Figure 3c are readily assigned to the ν_3, ν_4, and ν_6 vibronic structure of an electronic origin inferred to be at 34 823 cm^{-1}. The excited state is $^1I_6$ $b\Gamma_5$, because (i) the ν_6 vibronic structure is prominent (i.e., not Γ_1), (ii) the zero phonon line is not observed (i.e., not Γ_4), and (iii) the location is consistent with our energy level calculation. The $\Gamma_4 \rightarrow {}^1I_6$ $b\Gamma_5$ and $\Gamma_4 \rightarrow {}^1I_6$ $b\Gamma_5 + \nu_6$ transitions are prominent above ca. 20 K. A further electronic origin can be assigned to the intense band at 34 983 cm^{-1}, which, on the basis of the magnetic dipole intensity calculation corresponds to $\Gamma_1 \rightarrow {}^3P_1\Gamma_4$. The vibronic structure based upon this electronic origin is very weak. However, above 20 K, a hot band near 35 180 cm^{-1} is assigned to the $\Gamma_4 \rightarrow {}^3P_1\Gamma_4 + \nu_3$ transition. The $\Gamma_1 \rightarrow {}^3P_0\Gamma_1$ τ_{1u} vibronic sideband is also expected in this spectral region. Unassigned bands near 35 108 and 35 130 cm^{-1} are thus assigned to the 260 and 288 cm^{-1} components of ν_3, but the remaining structure is obscured by other transitions. The $^3P_0\Gamma_1$ electronic state is thus located at 34 846 cm^{-1}. At 30 K, two hot bands in this region remain unaccounted for, but they can then be assigned to the $\Gamma_4 \rightarrow {}^3P_0\Gamma_1$ and $\Gamma_4 \rightarrow {}^3P_0\Gamma_1 + \nu_6$ transitions.

The highest energy bands in Figure 3c, at 35 495, 35 472 cm^{-1} correspond to the 288 cm^{-1} components of ν_3, so that the corresponding electronic origins are then located at 35 207 and 35 184 cm^{-1}. Further structure can then be assigned to the other components of ν_3, as well as to the ν_4 vibronic origins, based upon the two electronic origins. The highest energy transition in this region is calculated to be $\Gamma_1 \rightarrow {}^1I_6\Gamma_1$, which cannot be split. By symmetry considerations, the 'splitting' of $\Gamma_1 \rightarrow {}^1I_6\Gamma_1$ is not due to a resonance with $\Gamma_1 \rightarrow {}^1I_6\Gamma_4 + \nu_2$, but could possibly be due to the resonance with $\Gamma_1 \rightarrow {}^1I_6\Gamma_4 + 2\nu_4$.

$^3P_2$ Term. The absorption spectrum of $Cs_2NaTmCl_6$ between 37 400 and 38 300 cm^{-1} is shown in Figure 3e. The bands are readily assigned to vibronic structure of the $\Gamma_1 \rightarrow {}^3P_2$ Γ_3, Γ_5 transitions.

Comparison with Two-Photon Excitation Spectra of $Cs_2NaYCl_6:Tm^{3+}$

The energy level assignments herein differ in some respects from those given in the two-photon spectral study of Thorne et al.[13] The major difference is that these authors did not take into account the electron−phonon coupling in the electronic ground state of $TmCl_6^{3-}$, which leads to the "doubling" of the $a\Gamma_5$ crystal field levels at $a\Gamma_5(1)$ 108 and $a\Gamma_5(2)$ 148 cm^{-1}. Thus, the unassigned band in the $^3H_6\Gamma_1 \rightarrow {}^3P_1\Gamma_4$ transition (at ca. 35 795 cm^{-1}) corresponds to $^3H_6$ $a\Gamma_5(1) \rightarrow {}^3P_1\Gamma_4$. By coincidence, the hot $a\Gamma_5(1) \rightarrow {}^1D_2$ transitions overlap with other hot band structure. However, two very weak bands in the $^3H_6\Gamma_1 \rightarrow {}^1D_2$ transition, near 27 696 and 27 786 cm^{-1} at 4 K, were unassigned. The first is presumably a resonance of $\Gamma_1 \rightarrow \Gamma_5 + S_5(\tau_{2g})$ with $\Gamma_1 \rightarrow \Gamma_3$, whereas the second corresponds to $\Gamma_1 \rightarrow \Gamma_5 + \nu_5(\tau_{2g})$ with the derived energy 130 cm^{-1}.

The $^3H_6\Gamma_1 \rightarrow {}^1I_6$ $a\Gamma_5$ transition was assigned at 34 167 cm^{-1} in ref 13, and there are hot bands at 56, 108, and 148 cm^{-1} to low energy. The $^1I_6$ Γ_2 level was not assigned, but was associated with two hot bands at ∼34 349, 34 403 cm^{-1}. Alternative assignments for these hot bands are to the first members of the ν_1 progression on the hot transitions $\Gamma_4 \rightarrow {}^1I_6$ $a\Gamma_5$ (34 059 cm^{-1}) and $a\Gamma_5(1) \rightarrow {}^1I_6$ $a\Gamma_5$ (34 111 cm^{-1}). It is uncertain whether there is also a peak near 34 224 cm^{-1}. We are unable to give a clear identification of the $^1I_6$ Γ_2 level from the combination of the one and two-photon data.

A major difference in the energy level assignments of Thorne et al.[13] and the present study concerns the $^1I_6$ Γ_1 level. This level was assigned to one (of two) very weak bands at 35 084 cm^{-1} in ref 13. On the basis of this assignment in the two-photon excitation spectra, we comment that although the $\Gamma_4 \rightarrow {}^1I_6\Gamma_1$ hot transition is unobserved (as expected) therein, the $a\Gamma_5(2) \rightarrow {}^1I_6\Gamma_1$ hot transition is coincident with the intense $\Gamma_4 \rightarrow {}^1I_6\Gamma_4$ transition and $a\Gamma_5(1) \rightarrow {}^1I_6\Gamma_1$ is not evident. The evidence for the assignment in ref 13 of $\Gamma_1 \rightarrow {}^1I_6\Gamma_1$ is thus weak, and in fact, the two very weak, broad bands observed (∼35 067 and 35 090 cm^{-1}) more likely correspond to $\Gamma_1 \rightarrow {}^1I_6b\Gamma_5 + \nu_2$, $\Gamma_1 \rightarrow {}^3P_0\Gamma_1 + \nu_2$, where the derived vibrational energy is 236 cm^{-1}. The alternative assignment proposed herein is supported by the two (unassigned) medium intensity bands at ca. 35 192, 35 214 cm^{-1} in ref 13. As expected, no hot $\Gamma_4 \rightarrow {}^1I_6\Gamma_1$ transition is apparent, but two other hot bands could correspond to $a\Gamma_5(1)$, $a\Gamma_5(2) \rightarrow {}^1I_6\Gamma_1$.

Energy Level Calculations

In their recent study,[13] Thorne et al. have presented an analysis of the electronic energy level structure of Tm^{3+} in Cs_2NaYCl_6. A crystal field analysis was performed including 37 experimental energy levels. The inadequacy of the standard Hamiltonian to reproduce the experimental energies in a satisfying way was emphasized. The mean experimental/

calculated deviation amounted to 55 cm^{-1} when all the levels were included in the calculation, to 36 cm^{-1} when the triplets were fitted separately, and to 22 cm^{-1} when only the singlets were involved. The fitted one-electron crystal field parameter B_0^4 was >60% larger for the singlets (2396 cm^{-1}) than for the triplets (1483 cm^{-1}). The $^1I_6$ levels were the most badly fitted, but were rather well simulated by a linear expansion of the first-order multiplet splitting. The use of SCCF parameters with a negative c^k coefficient produced a similar effect by providing a stronger crystal field for the singlets than for the triplets. Utilizing 14 parameters, the standard deviation decreased down to 28.2 cm^{-1}.The values of the energy levels of Cs_2NaYCl_6:Tm lower than 27 000 cm^{-1} utilized by Thorne et al. originated from earlier work on $Cs_2NaTmCl_6$.

In this work, as mentioned above, some changes were made both in the energies and in the ordering of levels. Besides minor calibration differences, altogether five energy levels in the present dataset are significantly different from those in ref 13. Since the assignments of the $^1I_6$, $^3F_3\Gamma_2$ levels are not secure, we have omitted these levels from our fits.

The $4f^{12}$ calculation on the basis of the 91 basis states of Tm^{3+} was first performed with the standard Hamiltonian including the usual interactions:[36,37] the electrostatic two-electron repulsion (parameters: F^2, F^4, F^6); the free-ion interconfiguration interaction (parameters: α, β, γ); the magnetic interaction (parameters: M^k, with $M^2 = 0.56M^0$ and $M^4 = 0.38M^0$); the spin−orbit interaction (parameter: ζ_f); the electrostatically correlated spin−orbit interaction (parameters P^k, with $P^4 = 0.75P^2$ and $P^6 = 0.50P^4$); and the crystal field interaction (parameters: B_0^4(f, f) and B_0^6(f, f), with $B_4^4(f, f) = \pm(5/14)^{1/2}B_0^4(f, f)$ and $B_4^6(f, f) = \mp (7/2)^{1/2} B_0^6(f, f)$ for the octahedral symmetry site). Using these 12 parameters, the mean deviation between experimental and calculated datasets was 53.3 cm^{-1}, being a similar value to that obtained by Thorne et al. The calculated energy levels are listed in Table 2 (calc 1), together with the experimental energies and the corresponding irreps. In Table 3 the parameters of the calculation are reported, as well as the corresponding mean and standard deviation. The ($^1D_2 + {}^3P_2$) and ($^3P_2 + {}^1D_2$) levels are surprisingly well fitted compared with the other levels.

We then applied to our dataset the model utilized in ref 13. It consists of modifying selectively the reduced matrix elements of U^4 and U^6 for triplet states. Actually, these are multiplied by $(1 + c^k)$, and the fitted values of c^4 and c^6 are equal to −0.42 and −0.33, close to the values obtained by Thorne et al. and listed in Table 2 of their paper.[13] The mean deviation decreases to 25.0 cm^{-1}, thus reducing the initial value by more than 2. However, the ($^1D_2 + {}^3P_2$) levels at 27 653 cm^{-1} (Γ_5) and 27 702 cm^{-1} (Γ_3) are fitted rather worse since the calculated $\Gamma_3(E_g)$ (27 636 cm^{-1}) and $\Gamma_5(T_{2g})$ (27 705 cm^{-1}) levels are inverted, in contradiction with the conclusions of the two-photon experiments and with the listing in Table 1 of ref 13.

Our goal is to obtain even better results by using a different method. This is achieved by utilizing full configuration interaction. We are not alluding to all possible interactions with all possible configurations but to a complete interaction with a few (preferably one) neighboring excited configurations. In a previous study,[38] we have shown that the crystal field analysis of Tm^{3+} ($4f^{12}$) datasets was improved when performing the fit in the enlarged basis $4f^{12}5p^6 + 4f^{13}5p^5$. The interacting configuration results from the gain of an electron by the 4f orbital and the loss of one electron by the complete $5p^6$ orbital. For $LuPO_4$, YPO_4, and LaOBr hosts the improvement (decrease of the mean deviation) amounts to 25, 17, and 40%, respectively. The improvement seems to be related to the relative strength of the fourth-order crystal field.

The same process is attempted in the present case for $Cs_2NaTmCl_6$, for which 37 energy levels out of 40 have been experimentally determined. The interactions within f^N (or p^M) can be calculated in $4f^{14-N}$ (or p^{6-M}) provided the signs of the one particle parameters are changed. The interactions within $4f^{12}np^6 + 4f^{13}np^5$ are formally the same as in the complementary system $4f^2mp^0 + 4f^1mp^1$ which involves 91 + 84 = 175 levels. This is just the interaction matrix which was considered earlier for Pr^{3+}.[13] The $4f^{12}np^6$ configuration contains levels with the same labels and the same degeneracies as $4f^2mp^0$, ($^1S_0$, $^1D_2$, $^1G_4$, $^3P_{0,1,2}$, $^3F_{2,3,4}$, $^3H_{4,5,6}$) and the same can be stated for the $4f^{13}np^5$ configuration with respect to $4f^1mp^1$, which contains $^1D_2$, $^1F_3$, $^1G_4$, $^3D_{1,2,3}$, $^3F_{2,3,4}$, and $^3G_{3,4,5}$. Although the earlier study[38] was performed with the assumption that the interacting configuration was $4f^{13}5p^5$, more recent evidence from the energy level fit of $Cs_2NaErCl_6$[15b] indicates that the configuration interaction involves contributions from the ligand, rather than from the metal ion, p-orbitals. The present work reinforces this important distinction.

The additional interactions which are to be taken into account within the larger matrix $4f^{12}np^6 + 4f^{13}np^5$ are: (i) the gap $\Delta E_{avg} = E'_{avg} - E_{avg}$, which determines the distance between the two configurations; (ii) the interconfiguration interaction (parameters: $R^k(4f, l_2, l_3, l_4)$, $k = 0, 2, 4$, with l_2, l_3, l_4 = 4f or np); (iii) the spin−orbit interaction (parameter: ζ_p); and (iv) the crystal field interaction (parameter: B_0^4(f, p)). The starting values were those for the metal ion $4f^{12}5p^6 + 4f^{13}5p^5$ systems. Theoretical parameter values calculated with Cowan's program RCN31[39] are (in cm^{-1}): $\Delta E_{avg} = 207\,403$; $\zeta_p = 32\,000$; R^2(f, p, f, p) = 55 952 (direct); R^2(f, p, p, f) = 27 980, R^4(f, p, p, f) = 21737 (exchange); R^2(f, f, f, p) = −14 616 and R^4(f, f, f, p) = −6554 (hybrid integrals). To keep the number of additional parameters as low as possible, a unique parameter X is included to scale the R^k integrals. This makes a total of 16 parameters, i.e., four more than in the $4f^{12}$ analysis and two more than in the SCCF calculation of Thorne et al. We shall comment on this point later. Taking into account the earlier studies, the starting value of B_0^4(f, p) was set equal to 10 times B_0^4(f, f).[38]

When utilizing the theoretical values for the gap, the R^k integrals ($X = 1$) and $\zeta_p = 32\,000$ cm^{-1}, no improvement of the fit could be achieved, whatever the value of B_0^4(f, p). The lowest mean deviation was 57 cm^{-1}, i.e., slightly worse than in the $4f^{12}$ analysis, with a fitted value of $B_0^4(f, p) = 22\,000$ cm^{-1}. The $4f^{13}5p^5$ configuration extends approximately from 2×10^5 up to 2.7×10^5 cm^{-1}. However, if X and ζ_p are allowed to vary freely, both parameters decrease dramatically as well as the mean deviation. Actually, by fixing ζ_p equal to 1000 cm^{-1} and letting X vary from 0.08 to 0.06, the dataset can be fitted with a mean deviation δ lower than 11 cm^{-1} for $31\,500 < \Delta E_{avg} < 10^5$ cm^{-1}. Beyond $\Delta E_{avg} = 10^5$ cm^{-1}, δ still increases moderately (13 cm^{-1} at 207 000 cm^{-1}) but B_0^4(f, p) reaches enormous values (−90 000 cm^{-1}). Figure 4 shows the variations of δ, B_0^4(f, f), B_0^6(f, f), B_0^4(f, p), and X as a function of ΔE_{avg}. The approximate value of the $4f^{12}$ barycenter is equal to 17 800 cm^{-1}. We note that the signs of B_0^4(f, f) and B_0^6(f, f) change for ΔE_{avg} approximately equal to 60 000 cm^{-1}. The smallest mean deviation is equal to 9.3 cm^{-1} and is obtained for $\Delta E_{avg} = 38\,500$ cm^{-1}. In this case, the whole $4f^{13}np^5$ configuration is inserted between the $^3P_2$ and $^1S_0$ levels of $4f^{12}$: between 54 000 and 66 000 cm^{-1}. The calculated energy levels are listed (calc 3) in Table 3. As already mentioned above, the best fit obtained

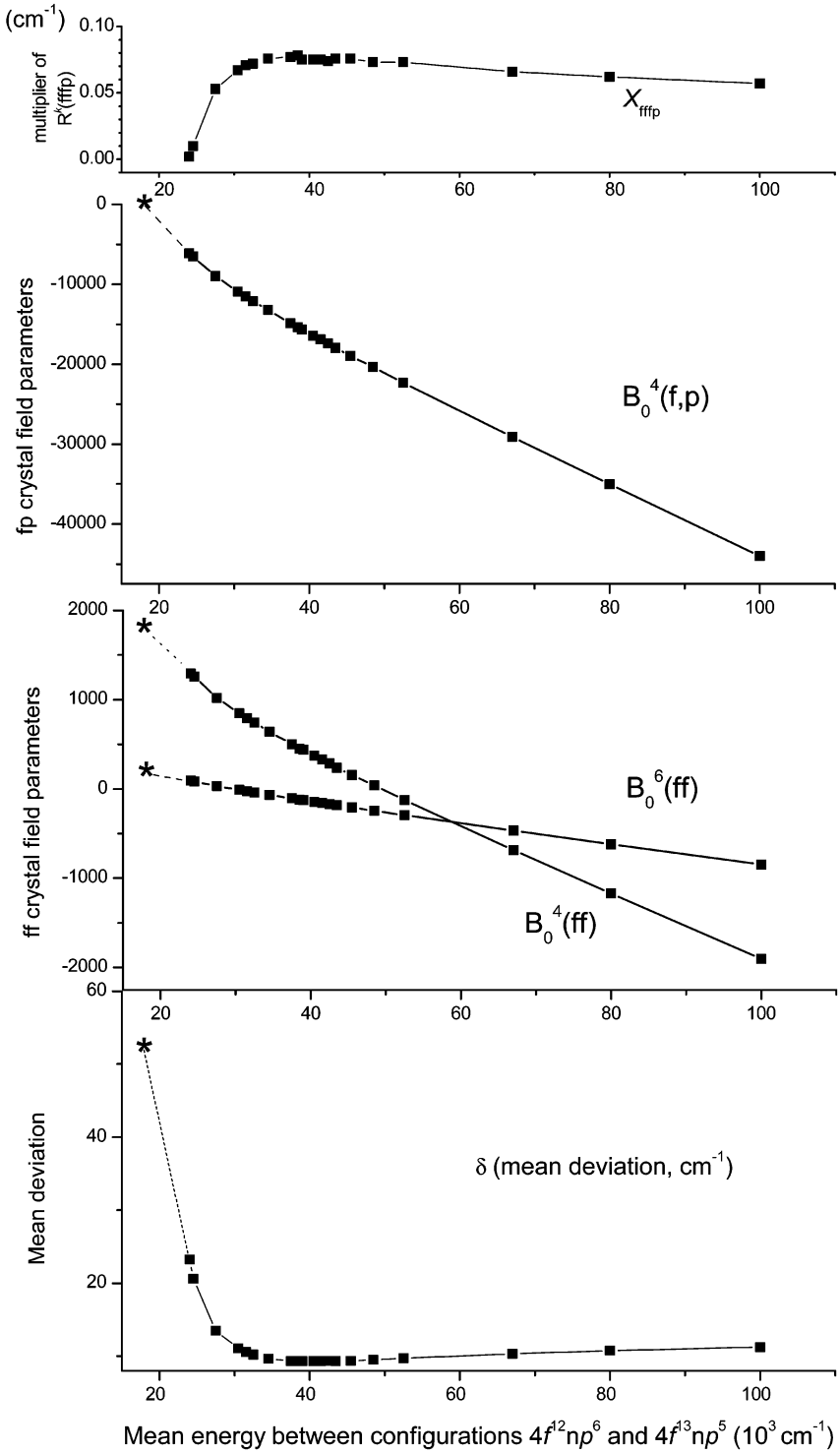

Figure 4. Plots of the various model parameters and mean energy deviation against the mean energy between the $4f^{12}np^6$ and $4f^{13}np^5$ configurations (10^3 cm^{-1}).

with the aid of the SCCF model on the same dataset produced a standard deviation equal to 25.0 cm^{-1}.

Table 4 lists the mean deviations within each *SLJ* level in calc 1, 2, and 3. In calc 1, the numbers between parentheses represent the barycentered deviations when they are very different from the nonbarycentered ones. This occurs mainly for $^1G_4$ and $^1I_6$ which are globally shifted: (-15 and $+20$ cm^{-1}, respectively). The largest deviations occur for $^3H_4$ and $^1I_6$ (65 and 92 cm^{-1}, respectively). Surprisingly, as noted above, ($^1D_2 + {}^3P_2$) and ($^3P_2 + {}^1D_2$) are rather well fitted. In calc 2 (SCCF) all the deviations have decreased except for ($^1D_2 + {}^3P_2$), where the Γ_3 and Γ_5 levels are now inverted. Finally, in calc 3, all the deviations have further decreased except for $^3H_4$ which remains bad from calc 1 to 3.

When the terms of $4f^{13}np^5$ are selectively withdrawn in turn from the interaction matrix, the fit worsens, the mean deviation rising each time up to 30−40 cm^{-1}. If X and ζ_p values are set equal to zero, the mean deviation increases up to 16 cm^{-1}.

Coming back to the best CI calculation (calc 3 in Table 3), all of the final $4f^{12}$ wave functions contain some admixtures with $4f^{13}np^5$ states. Those concerning the $^3H_6$, $^1D_2$, $^1I_6$, $^3P_0$, $^3P_1$, and $^3P_2$ wave functions are reported in Table 5. The admixture

TABLE 4: Mean Deviation δ within the SLJ Levels[a]

		δ (cm^{-1})		
$^{2S+1}L_J$	BC	$4f^{12}$ calc 1	$4f^{12}$ SCCF calc 2	$4f^{12}np^6 + 4f^{13}np^5$ calc 3
$^3H_6$	207	65	7	6
$^3F_4$	5754	42	36	5
$^3H_5$	8379	42	9 (6)	5
$^3H_4$	12 667	34	24	22
$^3F_3$,$^3F_2$[b]	14 441, 15 060	17	12	5
$^1G_4$	21 228	19 (12)	24 (21)	5
$^1D_2 + {}^3P_2$	27 673	12 (10)	58	4
$^3P_0$	34 846	23	10	0
$^1I_6$[b]	34 610	92 (90)	25	10
$^3P_2 + {}^1D_2$	37 697	14	14 (9)	11

[a] The values between parentheses refer to barycentered (BC) levels. [b] Incomplete terms.

TABLE 5: Percentage Admixture of $4f^{13}np^5$ States into $4f^{12}$

$4f^{12}$			$4f^{13}np^5$ levels							
level	irrep	energy	$^1D_2$	$^1F_3$	$^1G_4$	$^3D_3$	$^3F_4$	$^3G_3$	$^3G_4$	$^3G_5$
$^3H_6$	Γ_1	0					0.7			
	Γ_4	56					0.4			
	aΓ_5	123				0.2				0.3
	Γ_2	261				0.4				
	bΓ_5	370								0.1
	Γ_3	394					0.2			
$^1D_2$	Γ_5	27 702		0.3	0.8			0.5		
	Γ_3	27 781			1			0.4		
$^1I_6$	Γ_3	34 117	3.9							
	aΓ_5	34 158	3.3	0.7	0.1					
	Γ_2	(34 384)		3.8						
	bΓ_5	34 822	0.4	1.7						
	Γ_4	34 983		1.1	0.5					
	Γ_1	35 196			0.4					
$^3P_0$	Γ_1	34 846			1		0.3		2	
$^3P_1$	Γ_4	35 884					0.2	0.8	0.1	2.5
$^3P_2$	Γ_3	37 462			1.4				1	0.8
	Γ_5	37 854			0.4				0.4	1.5

is small for the lower levels, such as $^3H_6$, but even so, the effect on the energy levels is quite important. The admixture of singlet $4f^{13}np^5$states into the triplet $4f^{12}$ wave functions (for instance, 1% $^1G_4$ into $^3P_0$) is due to a $^1G_4 - {}^3G_4$ spin−orbit interaction in $4f^{13}np^5$ followed by a $^3P_0 - {}^3G_4$ interaction in $4f^{12}$.

The *SLJ* wave functions of $4f^{13}np^5$ are heavily mixed together. One difference which can be observed between the theoretical structure of $4f^{13}5p^5$ (calculated with $\Delta E_{avg} = 207\,403$ cm^{-1}, $\zeta_p = 32\,000$ cm^{-1}, and $X = 1$) and the final structure given by calc 3 is that in the former case, the $^1D_2$ levels are completely rejected at the top of the configuration while in the second case, large components are present in low-lying levels, close to $4f^{12}$.

We have still not firmly concluded about the nature of the interacting configuration. Considering the optimum value of ζ_p (its order of magnitude is 1000 instead of 32 000 cm^{-1}, but it is not possible to proceed to a real fitting) and X ($\cong 0.08$ instead of 1), it seems actually impossible for the interacting configuration to be $4f^{13}5p^5$ as was assumed in ref 38. As remarked in ref 15b, the p electrons involved in the process do not necessarily belong to the metal ion but might come from the neighboring chloride ions of the first coordination shell. It was indeed shown that the 3p wave function is partially projected on the central ion as a p function. This hypothesis is consistent with the present results as well as those obtained in ref 15b on $Cs_2NaErCl_6$. From now on, we shall refer to $4f^{13}np^5$ rather as an excited molecular orbital than an excited atomic configuration. The unconventional feature stands in the fact that we deal with it *as if it were* a central ion configuration.

Actually, the ultraviolet absorption spectrum of the sample shows a little hump, at the limit (∼200−210 nm, i.e., 47 600−50 000 cm^{-1}) of the instrument, which corresponds to a void zone in calc 3. However, we have seen that the curve representing δ, the mean deviation of the fitting, is quite flat for large variations of the gap. For $\Delta E_{avg} = 31\,500$ cm^{-1}, δ only increases up to 10.6 cm^{-1} and the excited configuration extends from 46 840 up to 58 529 cm^{-1} which is more compatible with the experiment. Then the structure of the excited configuration is as follows. Due to the large cubic crystal field parameter, it is grossly divided into two parts, comprising 48 and 36 levels. In the lower part, we find successively: between 46 840 and 47 400 cm^{-1}, 27 levels grouping essentially $^1F_3$, $^3F_4$, and $^3G_5$; at 48 300 cm^{-1}, five combinations of $^1D_2$ and $^3D_2$ levels; and between 48 500 and 49 200 cm^{-1}, $^3D_3$ and $^3G_4$ (16 levels). In the upper part, above a 6000 cm^{-1} gap, come $^1G_4$,$^3G_4$, $^1D_2$, $^3D_2$, $^3D_1$, $^3F_2$, $^1F_3$, $^3F_3$ (24 levels) between 55 800 and 57 200 cm^{-1}. Seven $^3G_3$ levels stand isolated at 57 800 cm^{-1}; a last bunch of five $^1D_2$ and $^3D_2$ levels at 58 500 cm^{-1} are at the top of the configuration.

Conclusions

From new electronic absorption and emission data, a revised energy level scheme for $Cs_2NaTmCl_6$ has been derived. The major discrepancies from previous studies have been resolved in terms of the interactions between pure electronic levels and gerade vibronic levels. The resulting dataset is poorly fitted when the calculation only comprises the 91-degenerate $4f^{12}$ levels, but is vastly improved when interactions with the $4f^{13}np^5$ configuration are included. It is impossible to assert that the perturbation of the $4f^{12}$ configuration is exercised by the $4f^{13}5p^5$ configuration since none of the parameters characterizing this configuration display the proper values. The spin−orbit coupling constant ζ_p has to be fixed to 1000 instead of 32 000 cm^{-1}, and X to 0.08 instead of 1. Both values are more than 1 order of magnitude smaller than those ascribed to a 4f/5p interaction. Now if the hole which has been assumed in the $5p^6$ orbital of $4f^{12}5p^6$, is rather a hole in the $3p^6$ orbital of a chloride ligand, then the lowering of the spin−orbit coupling constant is more understandable since the spin−orbit coupling constant of a p electron in $3p^6$ is about 500 cm^{-1}. Moreover, the interconfiguration parameters R^k(4f, 4f, 4f, 3p) are lower than R^k(4f, 4f, 4f, 5p) since the origin of one wave function is displaced on a ligand's site. Such an integral calculated at a 2.3 Å distance is of the order of 10^{-2} atomic units, i.e., 1000 cm^{-1}. Besides, our experimental laser excitation line data in Figure 2 indicate that the $4f^{13}np^5$ configuration lies in the region between 200 and 218 nm (50 000−45 870 cm^{-1}) and a value ∼46 800 cm^{-1} has been reported from absorption spectral data.[40] Ionova et al.[32] have assigned charge-transfer transitions in $TmCl_6^{3-}$ close to 210 nm (48 000 cm^{-1}). We therefore assume that the perturbation of the $4f^{12}$ configuration is actually exercised by a $4f^{13}3p^5$ configuration (and not $4f^{13}5p^5$), in which a ligand electron has been promoted into the 4f orbital. Indeed, with this new hypothesis, the fitted values of the three parameters: ΔE_{avg}, X, and ζ_p are close to the theoretical values. We do not expect the CT transition to be observed strong since it is electronically electric-dipole forbidden, and probably vibronic in nature, due to progression-forming modes arising from the bond length change.

Several authors have pointed out that the electron−phonon coupling strength is greatest for the early (Ce^{3+}, Pr^{3+}) and late (Tm^{3+}, Yb^{3+}) members of the lanthanide series.[41−43] The coupling strength is greatest when the metal ion wave functions

are most sensitive to movements of the ligand nuclei. This will happen when ligand-based states are mixed into the metal ion wave functions. We have found that this occurs most for the ions that are most easily oxidized (Ce^{3+}, Pr^{3+}) or reduced (Tm^{3+}, Yb^{3+}). Also, other members of the lanthanide series have more extended f^N configurations and intraconfigurational mixing is more important than interconfigurational mixing. The trend in electron−phonon coupling strengths along the series thus parallels the trends in mixing of charge-transfer configurations into lanthanide ion configurations. The mixing of more extended ligand p orbitals may also play a role in energy transfer phenomena such as exchange interactions.

In a recent paper, Judd and Lo[44] constructed an effective two-electron operator V_2 to simulate the effect of p-electron admixtures in f^N configurations. In cubic environments, this depends on just two parameters. V_2 is able to reproduce the trends obtained by a complete diagonalization. The authors point out that for the $4f^8$ configuration the contribution of $f \leftrightarrow f'$ (spin-correlated crystal field) interaction should be included as well.

Acknowledgment. P.A.T. thanks the City University of Hong Kong for financial support of this work under Strategic Research Grant No. 7001199.

References and Notes

(1) Morss, L. R.; Siegel, M.; Stinger, L.; Edelstein, N. *Inorg. Chem.* **1970**, *9*, 1771.
(2) Morrison, C. A.; Leavitt, R. P.; Wortman, D. E. *J. Chem. Phys.* **1980**, *73*, 2580.
(3) Richardson, F. S.; Reid, M. F.; Dallara, J. J.; Smith, R. D. *J. Chem. Phys*. **1985**, *83*, 3813.
(4) Tanner, P. A.; Kumar, V. V. R. K.; Jayasankar, C. K.; Reid, M. F. *J. Alloys Compds.* **1994**, *215*, 349.
(5) Reid, M. F.; Richardson, F. S.; Tanner, P. A. *Mol. Phys.* **1987**, *60*, 881.
(6) Jayasankar, C. K.; Richardson, F. S.; Reid, M. F.; Tanner, P. A. *Mol. Phys.* **1987**, *61*, 635.
(7) Denning, R. G.; Berry, A. J.; McCaw, C. S. *Phys. Rev.* **1998**, *B57*, R2021.
(8) Berry, A. J.; McCaw, C. S.; Morrison, I. D.; Denning, R. G. *J. Lumin.* **1996**, *66&67*, 272.
(9) Thorne, J. R. G.; Jones, M.; McCaw, C. S.; Murdoch, K. M.; Denning, R. G.; Khaidukov, N. M. *J. Phys. Condens. Matter* **1999**, *11*, 7851.
(10) Thorne, J. R. G.; Karunathilake, A.; Choi, H.; Denning, R. G.; Luxbacher, T. *J. Phys. Condens. Matter* **1999**, *11*, 7867.
(11) Berry, A. J.; Morrison, I. D.; Denning, R. G. *Mol. Phys.* **1998**, *93*, 1.
(12) Morrison, I. D.; Berry, A. J.; Denning, R. G. *Mol. Phys.* **1999**, *96*, 43.
(13) Thorne, J. R. G.; Zheng, Q.; Denning, R. G. *J. Phys. Condens. Matter* **2001**, *13*, 7403.
(14) McCaw C. S.; Denning, R. G. *Mol. Phys.* **2003**, *101*, 439.
(15) (a) Tanner, P. A.; Mak, C. S. K.; Faucher, M. D. *J. Chem. Phys.* **2001**, *114*, 10860. (b) Faucher, M. D.; Tanner, P. A. *Mol. Phys.* **2003**, *101*, 983.
(16) Meyer, G. *Prog. Solid State Chem.* **1982**, *14*, 141.
(17) Faucher, M. D.; Moune, O. K.; Garcia, D.; Tanner, P. *Phys. Rev.* **1996**, *B53*, 9501.
(18) Schwartz, R. W.; Faulkner, T. R.; Richardson, F. S. *Mol. Phys.* **1979**, *38*, 1767.
(19) (a) Tanner, P. A. *Mol. Phys*. **1984**, *53*, 813. (b) Tanner, P. A. *Mol. Phys.* **1984**, *53*, 835. (c) Tanner, P. A. *Mol. Phys.* **1985**, *54*, 883. (d) Tanner, P. A. *J. Chem. Soc., Faraday Trans. 2* **1985**, *81*, 1285.
(20) Foster, D. R.; Reid, M. F.; Richardson, F. S. *J. Chem. Phys*. **1985**, *83*, 3225.
(21) (a) Tanner, P. A. *J. Chem. Phys*. **1986**, *85*, 2344. (b) Richardson, F. S. *J. Chem. Phys.* **1986**, *85*, 2345.
(22) Ankudinov, A. L.; Dushin, R. B. *Phys. Solid State* **1995**, *37*, 865.
(23) Amberger, H.-D.; Rosenbauer, G. G.; Fischer, R. D. *J. Phys. Chem. Solids* **1977**, *38*, 379.
(24) Tanner, P. A.; Xia, S.; Liu, Y.-L.; Ma, Y. *Phys. Rev.* **1997**, *B55*, 12182.
(25) Mak, C. S. K.; Tanner, P. A.; Tröster, T.; Xia, S. *J. Phys. Chem. Solids* **2002**, *63*, 1623.
(26) Tanner, P. A.; Mak, C. S. K.; Kwok, W.-M.; Phillips, D. L.; Joubert, M. F. *J. Phys. Chem. B* **2002**, *106*, 3606.
(27) Knudsen, G. P.; Voss, F. W.; Nevald, R.; Amberger, H.-D. In *Rare Earths in Modern Science and Technology*; McCarthy, G. J., Silber, H. B., Rhyne, J. J., Eds.; Plenum: New York, 1982; Vol. 3, p 335.
(28) Bleaney, B.; Stephen, A. G.; Walker, P. J.; Wells, M. R. *Proc. R. Soc. London* **1982**, *A381*, 1.
(29) Lentz, A. *J. Phys. Chem. Solids* **1974**, *35*, 827.
(30) Tanner, P. A.; Siu, G. G. *Mol. Phys*. **1992**, *75*, 233.
(31) Tanner, P. A. *J. Mol. Struct.* **1997**, *405*, 103.
(32) Ionova, G.; Krupa, J. C.; Gérard, L.; Guillaumont, R. *New J. Chem.* **1995**, *19*, 677.
(33) Tanner, P. A.; Choi, T. K.; Hoffman, K. *Appl. Spectrosc.* **1993**, *47*, 1084.
(34) Kirk, A. D.; Furer, N.; Güdel, H. U. *J. Lumin.* **1996**, *68*, 77.
(35) Tanner, P. A.; Acevedo, R.; Hurtado, O.; Meruane, T. *J. Alloys Compds* **2001**, *323*−*324*, 718.
(36) Judd, B. R.; Crosswhite, H. *J. Opt. Soc. Am. B* 1984, *1*, 255.
(37) Judd, B. R. *Operator Techniques in Atomic Spectroscopy*; Princeton University Press: New York, 1998.
(38) Faucher, M. D. *Eur. Phys. J.* **1998**, *D3*, 9.
(39) Cowan, R. D. *Computer Program RCN31*; Los Alamos National Laboratory: Los Alamos, 1981.
(40) Blasse, G. *Struct. Bonding* **1976**, *26*, 43.
(41) Ellens, A.; Andres, H.; ter Heerdt, M. L. H.; Wegh, R. T.; Meijerink, A.; Blasse, G. *Phys. Rev*. **1997**, *B55*, 180.
(42) Campos, A. F.; Meijerink, A.; de Mello Donegá, C.; Malta, O. L. *J. Phys. Chem. Solids* **2000**, *61*, 1489.
(43) Lupei, A.; Lupei, V.; Enaki, V. N.; Presura, C.; Petraru, A. *Spectrochim. Acta* **1999**, *A55*, 773.
(44) Judd, B. R.; Lo, E. *Mol. Phys.* **2004**, *102*, 47.